JOURNAL OF Materials CHEMISTRY

X-Ray crystal structure, magnetic and electric properties of TTF trimer-based salts of $FeCl_4^-$, $[TTF_7(FeCl_4)_2]$†

Masanori Umeya, Satoshi Kawata, Hiroyuki Matsuzaka, Susumu Kitagawa,* Hiroyuki Nishikawa, Koichi Kikuchi and Isao Ikemoto

Department of Chemistry, Tokyo Metropolitan University, Minami-Ohsawa, Hachiouji, Tokyo, 192–03, Japan

A new TTF trimer-based charge transfer salt, $TTF_7(FeCl_4)_2$, has been synthesized and characterized. It belongs to the monoclinic space group $C2/m$, $M=1812.75$, $a=28.433(5)$, $b=16.524(3)$, $c=16.981(3)$ Å, $\beta=121.17(2)^\circ$, $V=6826(2)$ Å^3 and $Z=4$. The crystal structure shows the two types of layers O and I; the layer O is composed of two sets of TTF trimers orthogonal to each other, providing a two-dimensional interacting network of TTF molecules, while the layer I consists of TTF molecules and $FeCl_4$ anions. The $FeCl_4$ anions can interact magnetically with the TTF molecules in both the layers O and I because of the short S···Cl distance. Single-crystal temperature-dependent conductivity measurements show that this material is a semiconductor with a room-temperature conductivity of 0.055 S cm^{-1} and a thermal activation energy of 0.15 eV. The temperature dependence of magnetic susceptibilities indicates antiferromagnetic behavior based on $FeCl_4^-$ anions and radical cations. Two EPR signals were observed for the microcrystals; the broader signal afforded a large temperature dependence of the g value ranging from 2.15 (292 K) to 1.86 (5 K).

The development of metallic molecular crystals of charge-transfer salts has attracted considerable interest of solid-state chemists because of the remarkable variety of crystal structures and physical properties.[1] Among these synthetic efforts one of the most exciting challenges is to prepare a new molecular compound with interplay of magnetic and conducting properties. It is useful to take advantage of the ability of the conduction electrons of a molecular metal to couple localized magnetic moments *via* an indirect exchange mechanism. In molecular materials it is possible to build a hybrid material formed by a conducting part (typically, a TTF derivative) and by a magnetic part (typically, an inorganic d-transition metal complex). BEDT-TTF is such a candidate having various packing structures (α, β, θ, and so on), and often affording a metallic phase. Very recently, transition metal-based hybrid compounds of BEDT-TTF have been synthesized.[2–9] Among these compounds $(BEDT\text{-}TTF)_4(H_2O)[Fe(C_2O_4)_3]\cdot C_6H_5CN$[3] is the first molecule-based magnetic superconductor with BEDT-TTF layers alternating with inorganic layers of paramagnetic tris(oxalato)iron(III) anions. Another TTF derivative-based compound, $(BETS)_2FeCl_4$ [BETS = bis(ethylenedithio)-tetraselenafulvalene], has shown unusual magnetic behavior associated with an interaction between the BETS molecule and the $FeCl_4$ anion.[10] In these hybrid compounds, the packing structure and charge state of the organic cations greatly depend on the combination of the organic cation and transition metal complex anion, influencing the magnetic interaction between the transition metal complex anions *via* the organic cations. Therefore, it is important to explore crystal structures relevant to this interaction by changing both organic cations and/or transition metal complex anions. The packing modes of TTF salts reported are one-dimensional (1-D) stacking,[11,12] discrete dimer structure,[12,13] and two-dimensional (2-D) structure,[14–16] which consists of TTF trimers. The charge state of TTF molecule in these TTF trimers is +2/3. The conductor anions of d-transition metal complexes found in these TTF salts are $CoCl_4^{2-}$, $MnCl_4^{2-}$ and $ZnCl_4^{2-}$.[15] Accordingly, the variety of the crystal structures is associated with counter-anions. In order to design new materials composed of inorganic–organic substructures, it is important to investigate the relationship between counter-anions and the crystal structures well characterized by X-ray crystallography. Here, we report the synthesis, structure and properties of a new charged state compound derived from $[(FeCl_4)_2(\mu\text{-}C_2O_4)]^{4-}$ and TTF, which consists of two layers constituted by TTF trimer units and $FeCl_4^-$/TTF units.

† Presented at the 58th Okazaki Conference, Recent Development and Future Prospects of Molecular Based Conductors, Okazaki, Japan, 7–9 March 1997.

Experimental

All operations were carried out under an atmosphere of nitrogen by using standard Schlenk-tube techniques. Solvents were purified by conventional methods and distilled under nitrogen prior to use.

Synthesis of $TTF_7(FeCl_4)_2$

To a solution of 0.04 mmol (30 mg) of $(H_2trien)_2[(FeCl_4)_2(\mu\text{-}C_2O_4)]\cdot 2H_2O$[17] ($H_2trien$ = triethylenediammonium) in 10 ml of methanol was added a solution of 0.64 mmol (75 mg) of TTF in 10 ml of acetone. The reaction mixture was stirred for several minutes and then stood at room temperature for 4 weeks. Black needles and prisms were collected by filtration and easily separated by hand (yield: 20%). Analysis: found C, 27.69; H, 2.58; requires C, 27.63; H, 1.55%.

X-Ray data collection and structure determination

A prism crystal was glued on the top of a glass fiber. The structure at 243 K was determined by using the 2928 significant reflections ($|F_o|>3\sigma|F_o|$), which were collected on a Weissenberg-type Rigaku X-Ray imaging plate system (R-AXIS 4). The structure was solved by direct methods (Rigaku TEXSAN crystallographic software package of Molecular Structure Corporation). Full-matrix least-squares refinements were carried out with anisotropic thermal parameters for all non-hydrogen atoms. All the hydrogen atoms were located in a difference Fourier map and introduced as fixed contributors in the final stage of the refinement. Residuals at convergence are quoted on $|F|$.

Table 1 Crystallographic data for $TTF_7(FeCl_4)_2$

chemical formula	$C_{42}H_{28}Cl_8Fe_2S_{28}$
formula mass	1812.75
space group	$C2/m$ (no. 12)
a/Å	28.433(5)
b/Å	16.524(3)
c/Å	16.981(3)
β/degrees	121.17(2)
V/Å^3	6826(2)
Z	4
D_c/g cm^{-3}	1.78
$F(000)$	3664.00
T/K	243
λ(Mo-Kα)/Å	0.71069
μ(Mo-Kα)/cm^{-1}	16.3
$2\theta_{max}$/degrees	51.4
R^a	0.041
$R_w{}^b$	0.051
goodness of fit	1.504

$^aR = \sum||F_o|-|F_c||/\sum|F_o|$. $^bR_w = [\sum w(|F_o|-|F_c|)^2/\sum wF_o{}^2]^{\frac{1}{2}}$.

Table 2 Central C=C and C−S bond distances (Å) of TTF molecules A–G

type[a]	r_a	r_b	r_c	r_d	r_e
A	1.36(2)	1.756(6)	1.756(6)	1.756(6)	1.756(6)
B	1.36(2)	1.751(7)	1.751(7)	1.751(7)	1.751(7)
C	1.33(1)	1.754(9)	1.742(8)	1.750(9)	1.739(10)
D	1.33(2)	1.71(1)	1.73(1)	1.74(1)	1.76(1)
E	1.35(2)	1.752(8)	1.752(8)	1.734(8)	1.734(8)
F	1.34(2)	1.732(8)	1.732(8)	1.739(8)	1.739(8)
G	1.33(2)	1.755(7)	1.755(7)	1.757(7)	1.757(7)

[a]The labels A–G correspond to those of TTF molecules in Fig. 2(*a*) and (*b*).

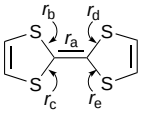

Table 3 Bond distances (Å) and angles (degrees) for $FeCl_4{}^-$

Fe(1)−Cl(1) 2.290(3)	Cl(1)−Fe(1)−Cl(2) 105.9(1)
Fe(1)−Cl(2) 2.326(3)	Cl(1)−Fe(1)−Cl(4) 105.9(1)
Fe(1)−Cl(3) 2.311(3)	Cl(1)−Fe(1)−Cl(3) 117.5(1)
Fe(1)−Cl(4) 2.308(3)	Cl(2)−Fe(1)−Cl(4) 120.1(1)
	Cl(2)−Fe(1)−Cl(3) 103.3(1)
	Cl(3)−Fe(1)−Cl(4) 105.0(1)

A summary of the crystallographic data, anisotropic parameters, and selected bond distances and angles are listed in Tables 1–3, respectively.

Full crystallographic details, excluding structure factors, have been deposited at the Cambridge Crystallographic Data Centre (CCDC). See Information for Authors, *J. Mater. Chem.*, 1998, Issue 1. Any request to the CCDC for this material should quote the full literature citation and the reference number 1145/59.

Physical measurements

The resistivity of the samples was measured by the conventional four-probe method in the temperature range 80–300 K. Four 15 μm diameter gold wires bonded to the crystal with carbon conducting paint were used as current and voltage terminals.

EPR spectra were recorded at X-band frequency with a JEOL RE-3X spectrometer operating at 9.1 GHz over the temperature range 5–300 K. Resonance frequency was measured on an Anritsu MF76A microwave frequency counter. Magnetic fields were calibrated by an Echo Electronics EFM-2000AX NMR field meter. The EPR spectra were recorded with a modulation frequency of 100 kHz and modulation amplitude of 0.5 mT, throughout.

Table 4 Comparison of Fe−Cl bond distances and Cl−Fe−Cl angles in $FeCl_4{}^-$

compound	Fe−Cl/Å	Cl−Fe−Cl/degrees
$TTF_7(FeCl_4)_2$	2.290–2.326	103.3–120.1
$(BEDT\text{-}TTF)_2FeCl_4$[a]	2.174–2.186	107.7–110.2
$(\lambda\text{-}BETS)_2FeCl_4$[b]	2.166–2.178	107.1–113.5
$(\kappa\text{-}BETS)_2FeCl_4$[b]	2.174–2.193	107.7–112.7

[a]Ref. 4. [b]Ref. 10.

The magnetic susceptibility data were recorded over the temperature range 2–300 K at 0.1 T with a SQUID susceptometer (Quantum Design, San Diego, CA) interfaced with an HP computer system. All the data were corrected for diamagnetism which were calculated from Pascal's tables.

Laser Raman spectra were recorded with Ar^+ ion excitation (514.5 nm) using a Jasco R-600 spectrometer. A 90° scattering geometry was employed.

Results and Discussion

Crystal structure

The packing system of $TTF_7(FeCl_4)_2$ is similar to that of the $TTF_{14}(MCl_4)_4$ series.[15] The TTF molecules and $FeCl_4$ anions are shown in Fig. 1 with the labeling scheme. The crystal structure consists of alternating TTF trimer layers (type O) and $FeCl_4{}^-$/TTF layers (type I), both of which are parallel to the *bc* plane. The molecular arrangements of the two types of the layers are shown in Fig. 2(*a*) and (*b*). The side-view (down the *b*-axis) of these layers is shown in Fig. 2(*c*). The type I layer contains two crystallographically independent TTF molecules [labeled A and B in Fig. 2(*a*)] and one independent $FeCl_4$ anion. The formal composition of the type I layer is $TTF_ATTF_B(FeCl_4)_4$. The A- and B-type TTF molecules sit parallel to the *bc* plane. On the other hand, the layer O contains five crystallographically independent TTF molecules denoted C, D, E, F and G in Fig. 2(*b*), which form the two groups of trimers, (1) and (2), orthogonal to each other. The formal composition of the layer O is thus $TTF_CTTF_ETTF_FTTF_G(TTF_D)_2$.

The central C=C and C−S bond distances (r) for TTF molecules (A–G) are listed in Table 2. Generally oxidized TTF^{n+} $(0<n<1)$ molecules have the C=C distance ranging from 1.31 to 1.40 Å.[11,13,18] The observed distances r_a in Table 2 fall within the range of 1.33–1.36 Å indicative of a TTF^{n+} $(0<n<1)$ state. The r_a values for TTF_A and TTF_B in layer I show the longest distance of 1.36 Å, implying a TTF^+ state. On the other hand, those for TTF_{C-G} in layer O are close to each other, making the oxidation state assignment for each TTF molecule difficult. Thus, the charged state of each layer is considered as $[(TTF_A)(TTF_B)(FeCl_4)_4]^{2-}$ and $[(TTF_C)(TTF_E)(TTF_F)(TTF_G)(TTF_D)_2]^+$, respectively. The average charge state of TTF_{C-G} is $+1/6$.

The S···S distances in trimers (1) and (2) [linkages (iii) and (iv) in Fig. 2(*b*)] are 3.4–3.5 Å, which correspond well to those observed in usual one-dimensional (1-D) columns of TTF salts.[11,12] Moreover, the S···S distances between the trimers are also short enough [3.63–3.93 Å; linkage (vi) and (vii) in Fig. 2(*b*)] to give rise to an interacting network, resulting in two-dimensional sheets. Most charge transfer TTF salts synthesized so far have either 1-D columns[11,12] or discrete dimer structures.[12,13] The present compound has a new structure type of TTF trimer-based layers. On the other hand, the S···S distance of 5.163 Å [linkage (ii) in Fig. 2(*a*)] indicates the absence of interaction between TTF_A and TTF_B in layer I.

The bond distances and angles of $FeCl_4{}^-$ in Table 3 indicates

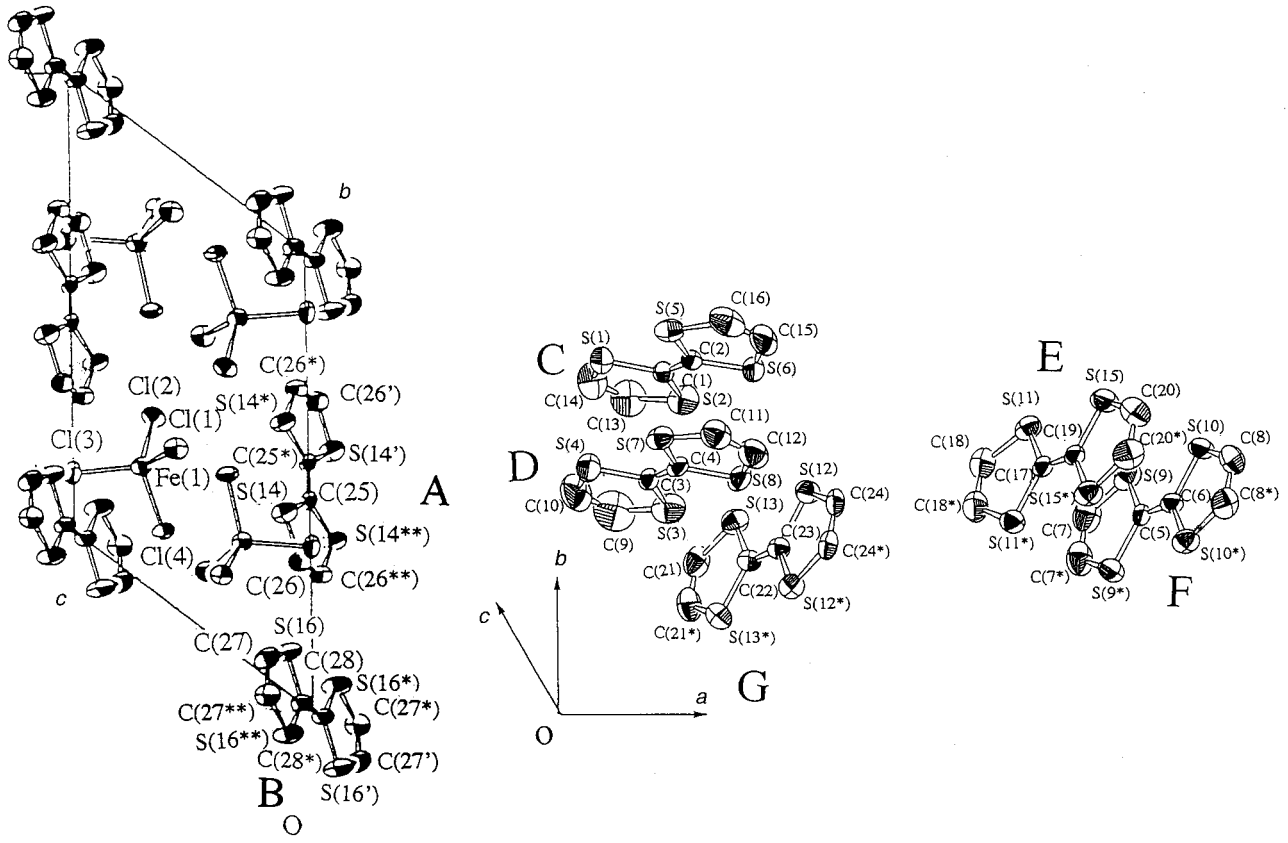

Fig. 1 Thermal ellipsoid drawings (50% probability) and numbering schemes for the seven crystallographically independent TTF molecules and $FeCl_4^-$ in $TTF_7(FeCl_4)_2$ [*Symmetry: $x, -y, z$; **symmetry: $-x, y, -z$; ′symmetry: $-x, -y, -z$]

a distorted tetrahedral geometry. As shown in Table 4, the deviation from tetrahedral is greater than those of the related charge transfer salts such as $(BEDT\text{-}TTF)_2FeCl_4$,[4] $(\lambda\text{-}BETS)_2FeCl_4$[10] and $(\kappa\text{-}BETS)_2FeCl_4$.[10]

The intriguing feature of this structure is the short S···Cl distances between the $FeCl_4^-$ anion and the TTF molecules. The interlayer S···Cl distance is 3.38 Å, which is shorter than the sum of the van der Waals radius of S and Cl atoms (3.65 Å). The intralayer S···Cl distances [linkage (i) in Fig. 2(*a*)] are 3.649–4.198 Å. On the other hand, an interesting magnetic interaction between the $FeCl_4^-$ anion and the BETS molecule was previously observed in $(\kappa\text{-}BETS)_2FeCl_4$,[10] the S···Cl distance of which was 3.54 Å, and one in $(BEDT\text{-}TTF)_2FeCl_4$ was 3.55 Å. The S···Cl distance of $TTF_7(FeCl_4)_2$, 3.38 Å, is even shorter than in these compounds. These short S···Cl distances are associated with a magnetic interaction between the π-spin of TTF radical cations and d-spin of $FeCl_4^-$ anions.

Physical properties

Four-probe dc transport measurements on $TTF_7(FeCl_4)_2$ reveal semiconducting behavior from 80 to 300 K with a room temperature conductivity σ_{RT} of 0.055 S cm^{-1} (Fig. 3). The activation energy varies smoothly from 0.15 eV at 300 K to 0.08 eV at 80 K, smaller at room temperature than, and comparable to, that of $TTF_7(MCl_4)_2$ (M = Co, Mn, Zn, Cd) [15,19,20] and $(BEDT\text{-}TTF)_2FeCl_4$.[4] The jump in the resistivity at *ca.* 280 K is probably due to cracking in the crystal.

The magnetic susceptibility was measured over the temperatures range 2–300 K (Fig. 4). $\chi_m T$ decreases at lower temperature and χ follows the Curie–Weiss law with a Weiss constant of −2.3 K and Curie constant of 0.23 emu K mol^{-1}. The magnetic moment at 300 K (5.81 μ_B) is much smaller than that expected on the basis of five unpaired electrons per Fe atom and one unpaired electron per TTF radical, indicative of the presence of antiferromagnetic interactions between TTF radicals and Fe ions. This is in contrast to the magnetic properties of $(BEDT\text{-}TTF)_2FeCl_4$,[4] whose magnetic moment is attributed to inorganic $FeCl_4^-$ anions.

Spectroscopic properties

The temperature dependence of the Raman bands is shown in Fig. 5. Three Raman bands at *ca.* 1500 cm^{-1} (1515, 1483, 1421 cm^{-1}), which are assigned to the central C=C stretching in the TTF molecule, were observed at 300 K. In the solid state, the ν_3 mode of the central C=C stretching occurs at 1512 cm^{-1} for TTF^0 and is seen at 1416 cm^{-1} in TTF^+.[21] On this basis, the Raman band at 1421 cm^{-1} is assigned to the TTF molecules A and B with +1 state, while the Raman bands at 1515 and 1483 cm^{-1} are assigned to the neutral TTF and partially oxidized $TTF^{n+}(0<n<1)$ for TTF molecules C–G. On the other hand, a new band (1446 cm^{-1}), which corresponds to the broad band (1200–1700 cm^{-1}) at 300 K, appeared at 72 K, suggesting the localization of charged states of TTF molecules by cooling.

The EPR spectrum of a polycrystalline sample in Fig. 6 consists of two types of signals [a sharp one (a) and a broad one (b)] in the entire temperature range (5–300 K). However the temperature dependence of the *g* values and their linewidths are completely different indicating that the signals arise from different radical cations or magnetic anions in the crystal. Signal (a) is much sharper than signal (b) and has no hyperfine structure. The mean *g* value, 2.007, which is attributed to a TTF radical, is unchanged upon decreasing the temperature (Fig. 7). The lineshape is isotropic at 292 K whereas it shows anisotropy at lower temperatures: an axial-symmetry pattern is observed above 50 K, while a rhombic pattern is observed below 50 K. These features suggest that signal (a) arises from

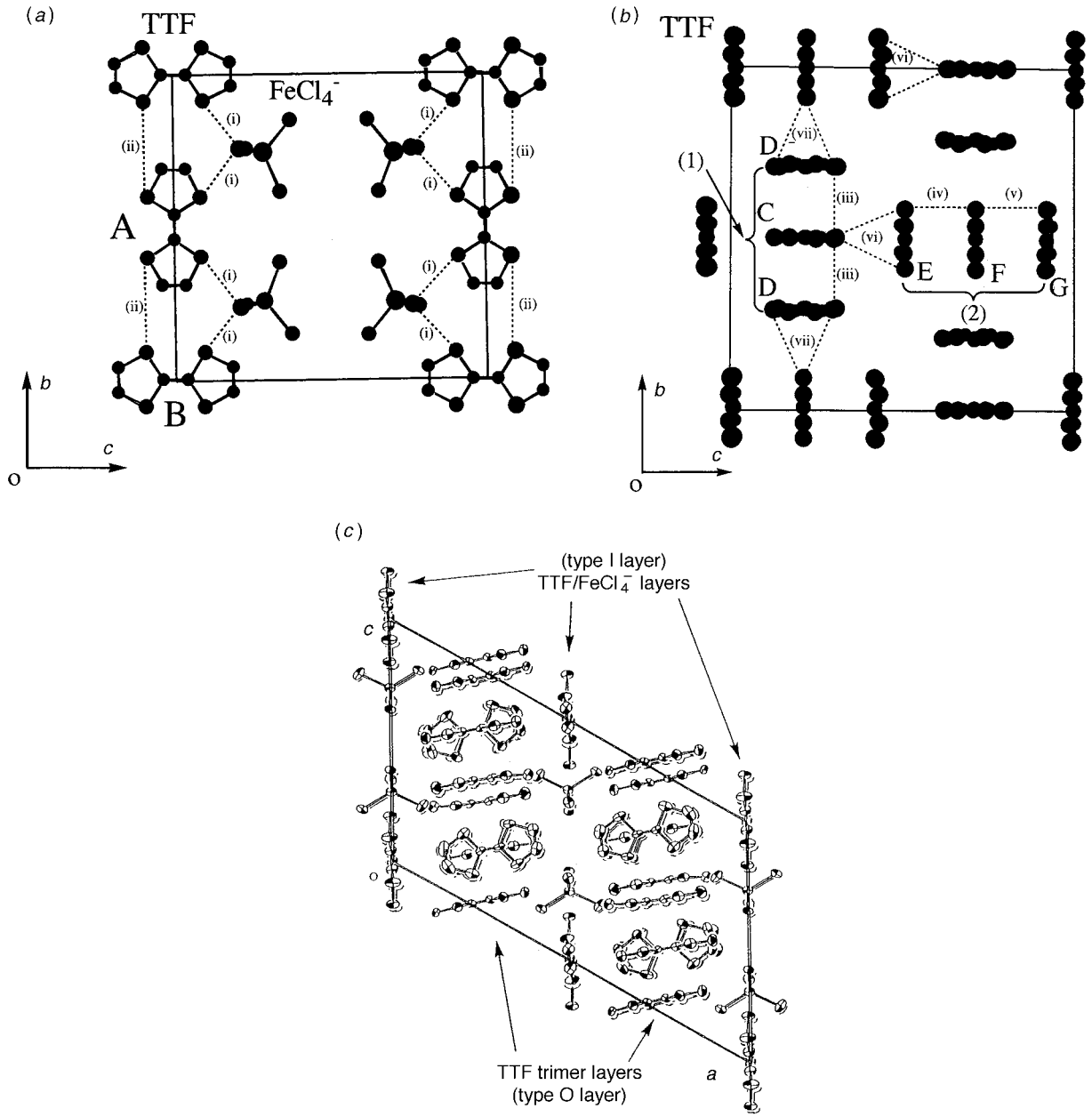

Fig. 2 (*a*) Projection of the $FeCl_4^-$/TTF layers (type I) along the *a*-axis. The dashed lines with the number indicate the short contact of S···Cl and S···S pairs. The distances are as follows: (i) 3.649–4.198 Å, (ii) 5.163 Å. (*b*) Projection of the TTF trimer layers (type O) along the *a*-axis. The dashed lines with the number indicate short S···S contacts. The distances are as follows: (iii) 3.474 Å, (iv) 3.476 Å, (v) 3.714 Å, (vi) 3.830–3.932 Å, (vii) 3.633–3.680 Å. (*c*) Projection of the TTF trimer layers (type O) and $FeCl_4^-$/TTF layers (type I) along the *b*-axis.

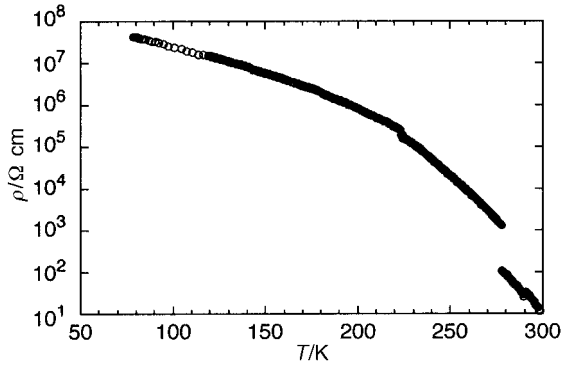

Fig. 3 Temperature-dependent resistivity of a single crystal of $(TTF)_7(FeCl_4)_2$

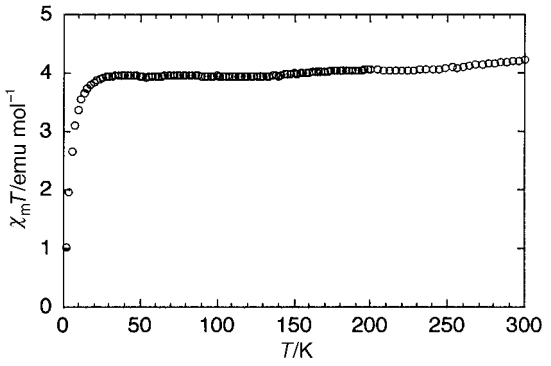

Fig. 4 $\chi_m T$ *vs.* T plot for $(TTF)_7(FeCl_4)_2$

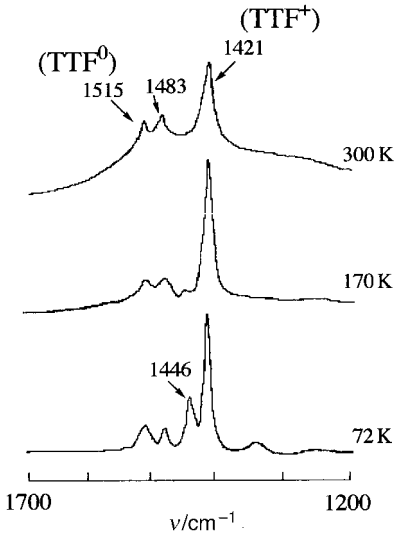

Fig. 5 Temperature dependence of Raman spectra of $(TTF)_7(FeCl_4)_2$

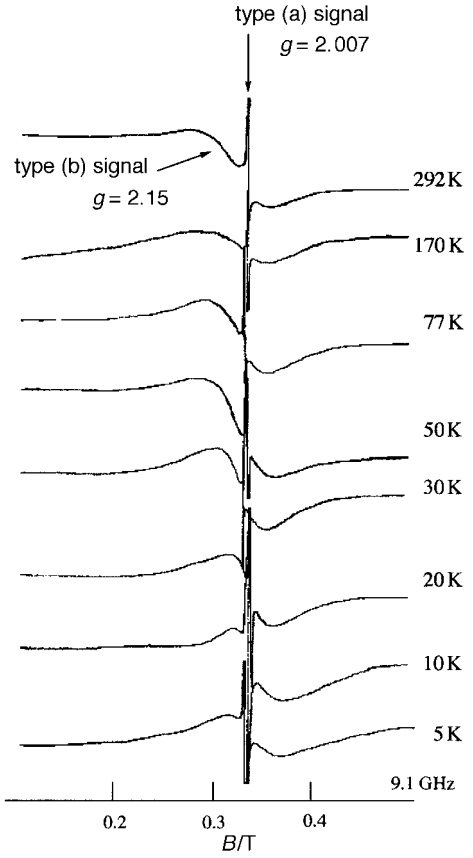

Fig. 6 Temperature dependence of EPR spectra of $(TTF)_7(FeCl_4)_2$. Type (a) and (b) indicate sharp and broad signals.

TTF^+ radicals displaying an exchange-coupled interaction. On the other hand, an apparent temperature dependence is observed for the signal (b). In $TTF_7(FeCl_4)_2$ the g value shifts from 2.15 at 292 K to 1.86 at 5 K and the peak-to-peak linewidth decreases with temperature (Fig. 7). The g value of signal (b) is larger than that for powdered $[Et_4N]FeCl_4$ ($g=2.025$) at high temperatures and smaller than that for the free electron ($g=2.0023$) at low temperatures, associated with the deviation from tetrahedral geometry of $FeCl_4^-$, thus implying an interaction between spins on Fe^{III} ions and TTF radicals. This unusual behavior in the EPR parameters was not observed for $(BEDT\text{-}TTF)_2FeCl_4$,[4] $(BETS)_2FeCl_4$,[10] $TTF(MnCl_3)_x$ ($x\approx0.75$), $TTF(MnCl_4)_x$ ($x\approx0.25$), or

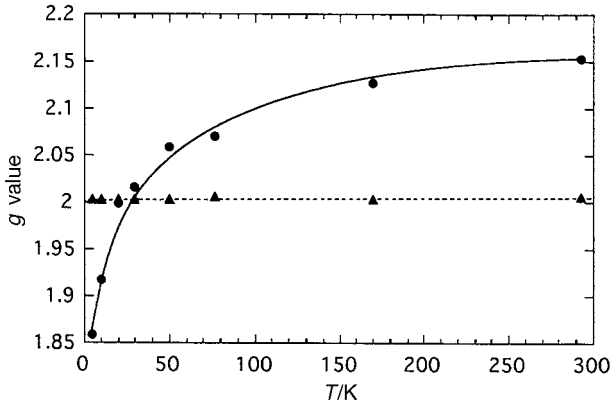

Fig. 7 Temperature dependence of the g-values of the two EPR signals of $(TTF)_7(FeCl_4)_2$. Black triangles and circles indicate the g-values of the type (a) and (b) signals, respectively, in Fig. 6.

$TTF(CoCl_4)_x$ ($x\approx0.25$).[20] The spin density of signal (b) is about ten times larger than that of signal (a) over the temperature range of 77–292 K. Consequently, signal (b) is associated with the two Fe^{III} ($S=5/2+5/2$) and one TTF radical ($S=1/2$) in $TTF_7(FeCl_4)_2$.

Conclusions

A TTF-based charge transfer salt, $TTF_7(FeCl_4)_2$, has been synthesized from the binuclear unit $[(Fe^{III}Cl_4)_2(\mu\text{-}C_2O_4)]^{4-}$, and is structurally characterized. The characteristic features are that $TTF_7(FeCl_4)_2$ is composed of three spin species, $FeCl_4^-$, $TTF_{A,B}$ and a TTF trimer. TTF_{C-G} molecules in type O layer have the charge state of 0 to +1. The d-spins in $FeCl_4$ anions and π-spins of TTF cation radicals, which sit close to each other, coexist in layer I. The crystal structure also reveals the occurrence of interlayer interactions of $FeCl_4$ anions and π-spins of TTF cation radicals. Finally, a temperature dependence of the g-values in the EPR signals is observed, characteristic of an interaction between the π-spin of TTF radicals and d-spin of $FeCl_4^-$ anions.

This work was supported by a Grant-in Aid for Scientific Research, the Ministry of Education, Science, Sports and Culture, Japan, and Nissan Foundation for the Promotion of Science.

References

1 M. Metzger, P. Day and G. C. Papavassiliou, *Lower-Dimensional Systems and Molecular Electronics,* Plenum Press, New York, 1990.
2 P. Day, M. Kurmoo, T. Mallah, I. R. Marsden, R. H. Friend, F. L. Pratt, W. Hayes, D. Chasseau, J. Gaultier, G. Bravic and L. Ducasse, *J. Am. Chem. Soc.*, 1992, **114**, 10 722.
3 M. Kurmoo, A. W. Graham, P. Day, S. J. Coles, M. B. Hursthouse, J. L. Caulfield, J. Singleton, F. L. Pratt, W. Hayes, L. Ducasse and P. Guionneau, *J. Am. Chem. Soc.*, 1995, **117**, 12 209.
4 T. Mallah, C. Hollis, S. Bott, M. Kurmoo and P. Day, *J. Chem. Soc., Dalton Trans.*, 1990, 859.
5 T. Mori, *Solid State Phys.*, 1991, **26**, 1.
6 C. J. Gomez-Garcia, L. Ouahab, C. Gimenez-Saiz, S. Triki, E. Coronado and P. Delhaes, *Angew. Chem., Int. Ed. Engl.*, 1994, **33**, 223.
7 C. J. Kepert, M. Kurmoo and P. Day, *Inorg. Chem.*, 1997, **36**, 1128.
8 C. J. Kepert, M. Kurmoo, M. R. Truter and P. Day, *J. Chem. Soc., Dalton Trans.*, 1997, 607.
9 C. J. Kepert, M. Kurmoo and P. Day, *J. Mater. Chem.*, 1997, **7**, 221.
10 H. Kobayashi, H. Tomita, T. Naito, A. Kobayashi, F. Sakai, T. Watanabe and P. Cassoux, *J. Am. Chem. Soc.*, 1996, **118**, 371.
11 L. Ouahab, M. Bencharif, A. Mhanni, D. Pelloquin, J.-F. Halet, O. Pena, J. Padiou and D. Grandiean, *Chem. Mater.*, 1992, **4**, 666.

12 B. A. Scott, S. J. L. Placa, J. B. Torrance, B. D. Silverman and B. Welber, *J. Am. Chem. Soc*., 1977, **28**, 6631.
13 R. C. Teitelbaum, T. J. Marks and C. K. Johnson, *J. Am. Chem. Soc*., 1980, **23**, 2986.
14 G. Matsubayashi, K. Ueyama and T. Tanaka, *J. Chem. Soc., Dalton Trans*., 1985, 465.
15 G. Maceno, Ch. Garrigou-Lagrange, M. Lequan, R. M. Lequan, J. Gaultier, F. Bechtel, G. Bravic and P. Delhaes, *Synth. Met*., 1988, **27**, B57.
16 K. Kondo, G. Matsubayashi, T. Tanaka, H. Yoshioka and K. Nakatsu, *J. Chem. Soc., Dalton Trans*., 1984, 379.
17 M. Feist, S. Troyanov and E. Kemnitz, *Inorg. Chem*., 1996, **35**, 3067.
18 M. Bousseau, L. Valade, J.-P. Legros, P. Cassoux, M. Garbauskas and L. V. Interrante, *J. Am. Chem. Soc*., 1986, **108**, 1908.
19 C. Garrigou-Lagrange, S. A. Rozanski, M. Kumoo and F. L. Pratt, *Solid State Commun*., 1988, **67**, 481.
20 M. Lequan, R. M. Lequan, C. Hauw, J. Gaultier, G. Maceno and P. Delhaes, *Synth. Met*., 1987, **19**, 409.
21 A. R. Siedle, T. F. Candela, A. G. Finnegan, R. P. V. Duyne, T. Cape and G. F. Kokoszka, *Inorg. Chem*., 1981, **20**, 2635.

Paper 7/03770H; *Received* 30*th May*, 1997